Condensation in Streamwise Vortex

Satoru Yamamoto
Dept.of Aeronautics and Space Engineering, Tohoku University
Aobayama01, Aoba-ku, Sendai 980-8579, Japan

Condensation observed in streamwise vortices generating from the leading edge of a double-delta wing in atmospheric flight conditions is numerically investigated. Three-dimensional laminar flows around the 76° -60° sharp-edged double-delta wing without thickness in atmospheric flight and wind tunnel conditions are calculated as the free-stream Mach number and the wing angle of attack are varied. The calculated results present that the onset of condensation in the streamwise vortex is very sensitive to flow conditions, especially the wing angle of attack.

1. Introduction

The actual atmosphere of the earth includes a finite amount of water vapor. It plays an important role in weather conditions and in the earth's various environments. Water vapor also plays an interesting role in the flight of airplanes. Water vapor may condense around an airplane. This is the so-called " vapor trail". Vapor trails are occasionally observed in the take-off, landing, and transonic cruising of airplanes. A vapor trail appears as a white cloud over the wing or extending from the wing tip. Campbell, Chambers and Rumsey[1] summarized a number of photographs of natural condensation. Condensation in atmospheric weather conditions is of fundamental interest in physics and it is a serious and unresolved problem also in the flight of airplanes. As a result, since condensation increases temperature and pressure due to the release of the latent heat of water associated with the phase change, the aerodynamic performance of an airplane varies considerably by condensation. A typical onset of condensation around the wing of an airplane is started by a rapid expansion of the flow in the supersonic region in atmospheric wind tunnel conditions. The flow is expanded from the leading edge of the wing. A huge amount of nucleus is produced from pure water vapor at a sufficiently high supersaturated condition. In atmospheric flight conditions, on the other hand, the chord length of wings is much longer than that of wind tunnel models. This reduces the cooling rate relative to the rate in wind tunnel experiments. Also, since the free stream is unsaturated, the region of supersaturation around the wing is locally restricted. Consequently, the rate of condensation in wind tunnel conditions may be overestimated compared to that in flight conditions. Furthermore, small particulates, such as dust, soot, ions and aerosols, in atmospheric humid air may play the role of the nucleus for the heterogeneous process. Therefore, the actual mechanism of condensation in flight is expected to be very complicated. Two-dimensional transonic flows of moist air around the airfoil in atmospheric wind tunnel conditions have been experimentally and numerically studied by Schnerr and Dohrmann[2]. The experimental Schlieren photographs present a condensation shock associated with the heat release of water ahead of an intrinsic shock wave. This indicates that the heating effect must be significant in this flow problem. Transonic viscous flows of moist air around NACA0012 airfoil in atmospheric wind tunnel conditions have been studied by Iriya, Yamamoto and Daiguji[3]. Three-dimensional transonic viscous flows around the ONERA M6 wing in atmospheric wind tunnel conditions have been calculated by Yamamoto, Hagari, and Murayama[4]. The phase of water liquid has been successfully visualized as a vapor trail around the wing. In this study, the computational code is applied to the calculation of condensation in a streamwise vortex produced over a double-delta wing in atmospheric flight conditions. As numerical examples, three-dimensional laminar flows around the 76° -60° sharp-edged double-delta wing without thickness in atmospheric flight and wind tunnel conditions are calculated under varying free-stream Mach numbers and wing angles of attack. The onset and the rate of condensation in each flow condition are compared with each other.

2. Fundamental Equations

The fundamental equations of three-dimensional compressible viscous flows in humid air consist of conservation laws of the total density, the momentums, the total energy, the density of water vapor, the density of water liquid, and the number density of nucleus. A homogeneous flow without velocity slips among air, water vapor and water liquid is solved by assuming as water droplets are sufficiently small. Flows around a delta wing in this study are supposed to be laminar flows for simplifying the present discussion on the calculated results, because the correlation between condensation and turbulence is still unknown. The system of equations is written in a vector form by

$$\partial Q/\partial t + \mathcal{F}(Q) = \frac{\partial Q}{\partial t} + \frac{\partial F_i}{\partial x_i} + S = 0 \qquad (1)$$

where

$$Q = \begin{bmatrix} \rho \\ \rho u_1 \\ \rho u_2 \\ \rho u_3 \\ e \\ \rho_v \\ \rho\beta \\ \rho n \end{bmatrix}$$

$$F_i = \begin{bmatrix} \rho u_i \\ \rho u_1 u_i + \delta_{i1} p - \tau_{i1} \\ \rho u_2 u_i + \delta_{i2} p - \tau_{i2} \\ \rho u_3 u_i + \delta_{i3} p - \tau_{i3} \\ (e+p)u_i - \tau_{ik}u_k - \kappa \partial T/\partial x_i \\ \rho_v u_i \\ \rho\beta u_i \\ \rho n u_i \end{bmatrix}$$

$$S = - \begin{bmatrix} 0 \\ 0 \\ 0 \\ 0 \\ 0 \\ -\Gamma \\ \Gamma \\ \rho I \end{bmatrix}$$

where, Q, F_i and S are the vectors of unknown variables, the flux components, and the sources. t and x_i are the time and the cartesian coordinates. ρ, u_i, e, ρ_v, β, and n are the total density, the physical velocity components, the total internal energy, the density of water vapor, the mass fraction of water liquid, and the number density of nucleus. p, τ_{ij}, κ, T, Γ, and I are the pressure, the stress tensors, the heat conductivity, the temperature, the mass generation rate due to condensation, and the nucleation rate. In this study, Eq.(1) is transformed to the system equation in general curvilinear coordinates (ξ_1 ξ_2 ξ_3). It is written by

$$\frac{\partial \hat{Q}}{\partial t} + \frac{\partial \hat{F}_i}{\partial \xi_i} + \hat{S} = 0 \qquad (2)$$

where

$$\hat{Q} = JQ, \quad \hat{F}_i = J(\partial \xi_i/\partial x_j)F_j, \quad \hat{S} = JS$$
$$J = \partial(x_1\ x_2\ x_3)/\partial(\xi_1\ \xi_2\ \xi_3)$$

The equations of a state of pressure and the speed of sound in this study have been derived by Ishizaka, Ikohagi and Daiguji[5], assuming as the mass fraction of water liquid β is sufficiently small($\beta < 0.1$). These equations are given by

$$p = \rho RT(1-\beta) \qquad (3)$$
$$c = \left[\frac{C_{pm}}{C_{pm} - (1-\beta)R} \frac{p}{\rho}\right]^{1/2} \qquad (4)$$

where

$$R = \left(\frac{\rho_a R_u}{\rho_g M_a} + \frac{\rho_v R_u}{\rho_g M_v}\right)$$

ρ_a and ρ_g are the densities of dry air and mixed gas. M_a, M_v are the molecular weights of dry air and water vapor. R_u is the universal gas constant. C_{pm} is defined by the linear combination of the specific heat at constant pressure between gas phase and liquid phase using β. The stress tensor τ_{ij} is given by

$$\tau_{ij} = \mu\left[\left(\frac{\partial u_i}{\partial x_j} + \frac{\partial u_j}{\partial x_i}\right) - \frac{2}{3}\delta_{ij}\frac{\partial u_k}{\partial x_k}\right] \qquad (5)$$

The molecular viscosity μ is also derived from the linear combination between that of gas phase and that of liquid phase using the mass fraction of liquid phase β.

3. Condensation Model

The homogeneous nucleation rate has been defined by Frankel[6]. This has been further modified by Kantrowitz[7]. This modified equation is given by

$$I = \frac{q_c}{1+\theta}\left(\frac{2\sigma}{\pi M_\ell^3}\right)^{1/2}\frac{\rho_g^2}{\rho_\ell}\exp\left(-\frac{4\pi r_*^2 \sigma}{3kT}\right) \qquad (6)$$

where q_c, σ, r_*, θ, M_ℓ, ρ_ℓ, and k are the condensation coefficient, the surface tension of a water liquid particle, the critical radius of nucleus, the correction parameter, the molecular weight of water liquid, the density of water liquid, and the Boltzmann constant. The critical radius of nucleus r_* is calculated by

$$r_* = 2\sigma/\rho_\ell RT\ln(s) \tag{7}$$

$s = p_v/p_s(T)$. s is the supersaturation ratio. p_v is the pressure of water vapor. $p_s(T)$ is the saturation pressure of water vapor at the local temperature T.

The mass generation rate Γ of water droplets consists of the mass generation rate of the critical-sized nuclei and the growth rate of the droplets. The mass generation rate Γ is approximated by

$$\Gamma = \frac{4}{3}\pi\rho_\ell I r_*^3 + 4\pi\rho_\ell n r^2 \frac{dr}{dt} \tag{8}$$

The mass fraction of water liquid β and the number density of nucleus n are calculated solving their conservation laws in Eq.(1). The growth rate of a water droplet dr/dt is described by the Hertz-Knudsen's law assuming as the droplet radius is much smaller than the mean free path of a vapor molecule.

4. Numerical Method

A high-resolution finite-difference method developed by our research group is used for solving the system of fundamental equations, Eq.(1). In this method, the fourth-order MUSCL extrapolation satisfying the TVD condition is implemented for the approximation of primitive variables[8]. The modified Roe's Riemann solver is also employed for space discretization of convection terms[9]. The viscosity term is calculated by the second-order central-difference scheme. The explicit second-order Runge-Kutta method is used for the time integration. The eight equations in Eq.(1) are solved simultaneously at each time step.

5. Numerical Examples

Laminar flows around the $76° - 60°$ sharp-edged double-delta wing in humid air are calculated. An atmospheric flight condition at low altitude is first specified. The uniform temperature, the uniform pressure, and the uniform relative humidity are fixed at 293.15[K], 1.24×10^5[Pa] and 90[%]. The Reynolds number is 1.4×10^6. Figure 1 plots the points where condensation is found or not found as the uniform Mach number and the angle of attack are changed. In the case of the angle of attack $\alpha = 10°$, no condensation occurs where the uniform Mach number $M_\infty < 0.7$. With the increment of the angle of attack, condensation is found at lower uniform Mach numbers. Although the angle of attack is changed from 10° to 30°, no condensation occurs at the uniform Mach number $M_\infty = 0.3$. No angle of attack beyond 30° was specified, because it is known that a vortex breakdown may occur and the flow becomes an unsteady turbulent flow. Consequently, the dashed line represents the boundary between the conditions with and without condensation.

The calculated density contours of water liquid at cross-flow sections are visualized in Figs.2-4 with streamlines indicating the strake vortex, the wing vortex and the tip vortex. Figure 2 presents the results with the uniform Mach number $M_\infty = 0.5$ and the angle of attack $\alpha = 20°$. Condensation starts from about 70% chord length in the strake vortex. A streamwise vortex is formed by the merging between the strake vortex and the wing vortex over the rear delta wing with the increase of the angle of attack. The amount of water liquid seems to be small and the wet region is local. Figure 3 presents the results with the uniform Mach number $M_\infty = 0.6$ and the angle of attack $\alpha = 20°$. The rate of condensation is drastically changed from Fig.2 despite a small increment of the uniform Mach number. Condensation starts from about 10% chord length in the strake vortex. The amount of water liquid is surprisingly larger than that of Fig.2. Also, the wet region is considerably wider than that in Fig.2. The wing vortex is merged with the strake vortex over the rear delta wing and then a streamwise vortex is produced. Furthermore, the tip vortex is merged with the streamwise vortex at the wake region. An interesting point is that the wet region spreads at the cross-flow section where these vortex mergings occur. Figure 4 presents the results of the uniform Mach number $M_\infty = 0.5$ and the angle of attack $\alpha = 30°$. The highest density of water liquid in this study is found locally in Fig.4. Condensation starts suddenly from about 20% chord length in the strake vortex. The high-density region of water liquid is intermediately located over the wing. However, the water liquid is suddenly evaporated near the trailing edge by the vortex breakdown.

Atmospheric wind tunnel conditions are next taken into consideration and compared with the previous results. In the case of the atmospheric

wind tunnel conditions, the stagnation temperature, the stagnation pressure and the inlet relative humidity are fixed at $T_0 = 293.15$[K], $p_0 = 1.24 \times 10^5$[Pa] and $\Phi = 90$[%]. The Reynolds number is $Re = 1.4 \times 10^6$. Figure 5 presents the calculated density contours of water liquid with the streamlines indicating the strake vortex, the wing vortex and the tip vortex. This figure is compared with Fig.2. The amount of water liquid increases drastically in the atmospheric wind tunnel conditions compared with that in the flight conditions. The onset point of condensation is located closely to the wing front, because the supersaturation ratio is estimated as higher in atmospheric wind tunnel conditions. Since the local temperature in the wind tunnel conditions is relatively lower than that in the flight conditions, the wet region starting from the onset point is maintained in the streamwise vortex far from the trailing edge. One interesting thing is that this result compare similarly with the results in Fig.3; that is, the 0.1 higher Mach number in the case of Fig.2.

6. Conclusions

Three-dimensional viscous flows around the 76°−60° sharp-edged double-delta wing in atmospheric flight conditions were calculated, and the condensation in the streamwise vortex, the so-called "vapor trail," was numerically investigated. The condensation is very sensitive to flow conditions. The onset of condensation depends on the uniform Mach number and the angle of attack. With the increase of these values, the condensation starts suddenly in the streamwise vortex.

References

1. Campbell, J.F., Chambers, J.R. and Rumsey, C.L., *J. Aircraft*, **26**, 1989, 593-604.
2. Schnerr, G.H. and Dohrmann, U., *AIAA J.*, **32**, 1994, 101-107.
3. Iriya, A., Yamamoto, S. and Daiguji, H. *Trans. JSME-B*,**62**, 1996, 100-105(in Japanese).
4. Yamamoto, S., Hagari, H. and Murayama, M., *Trans. JSASS*, **42**, 2000, 182-189.
5. Ishizaka, K, Ikohagi, T., and Daiguji, H., *Trans. JSME, Series B*, **60**, 1994, 3887-3892(in Japanese).
6. Frankel, J. Kinetic Theory of Liquids, 1955, Dover.
7. Kantrowitz, A., *J. Chemical Physics*, **19**, 1951, 1097-1100.
8. Yamamoto, S. and Daiguji, H., *Computers and Fluids*, **22**,1993, 259-270.
9. Yuan, X., Yamamoto, S. and Daiguji, H., *AIAA Paper* 94-3199, 1994.

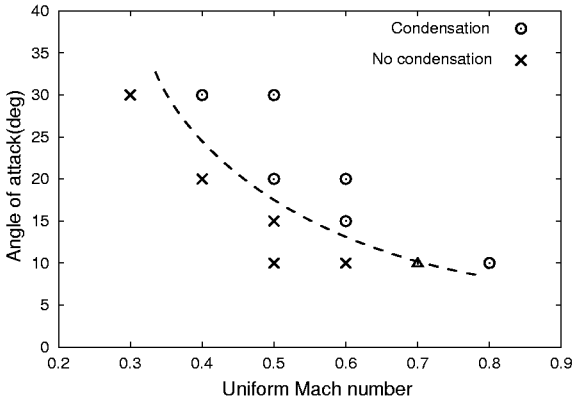

Fig. 1: Points where condensation is found or not found as uniform Mach number and angle of attack are changed

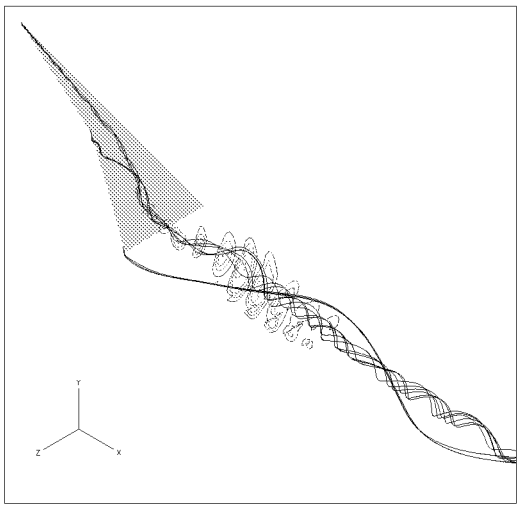

Fig. 2: Calculated density of water liquid at cross flow sections and the streamlines ($M_\infty = 0.5$ and $\alpha = 20°$)

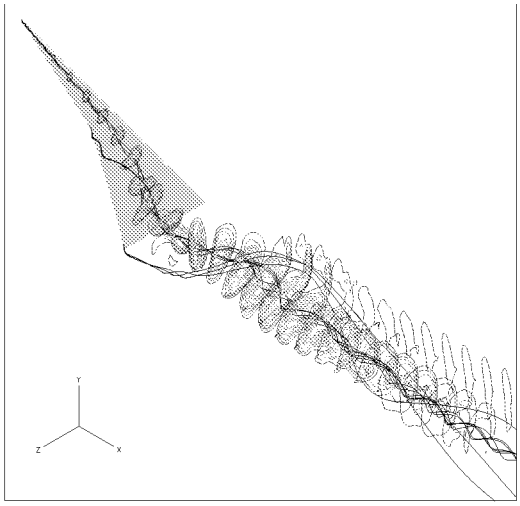

Fig. 3: Calculated density of water liquid at cross flow sections and the streamlines ($M_\infty = 0.6$ and $\alpha = 20°$)

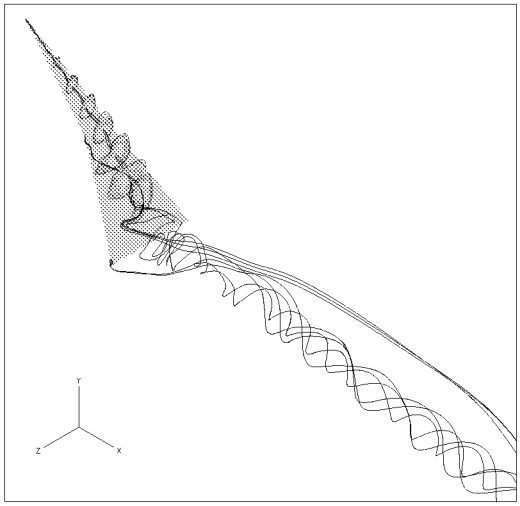

Fig. 4: Calculated density of water liquid at cross flow sections and the streamlines ($M_\infty = 0.5$ and $\alpha = 30°$)

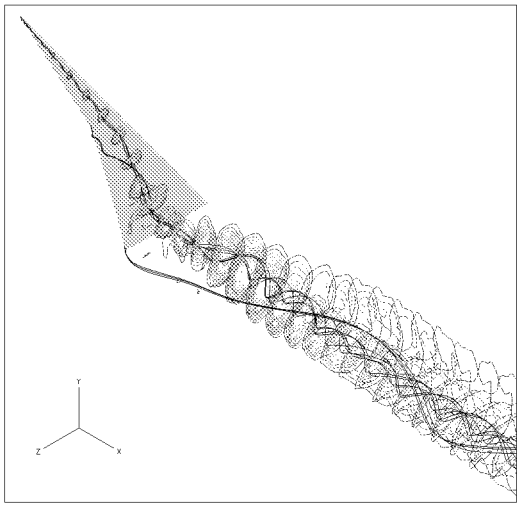

Fig. 5: Calculated density of water liquid at cross flow sections and the streamlines (atmospheric wind tunnel condition)